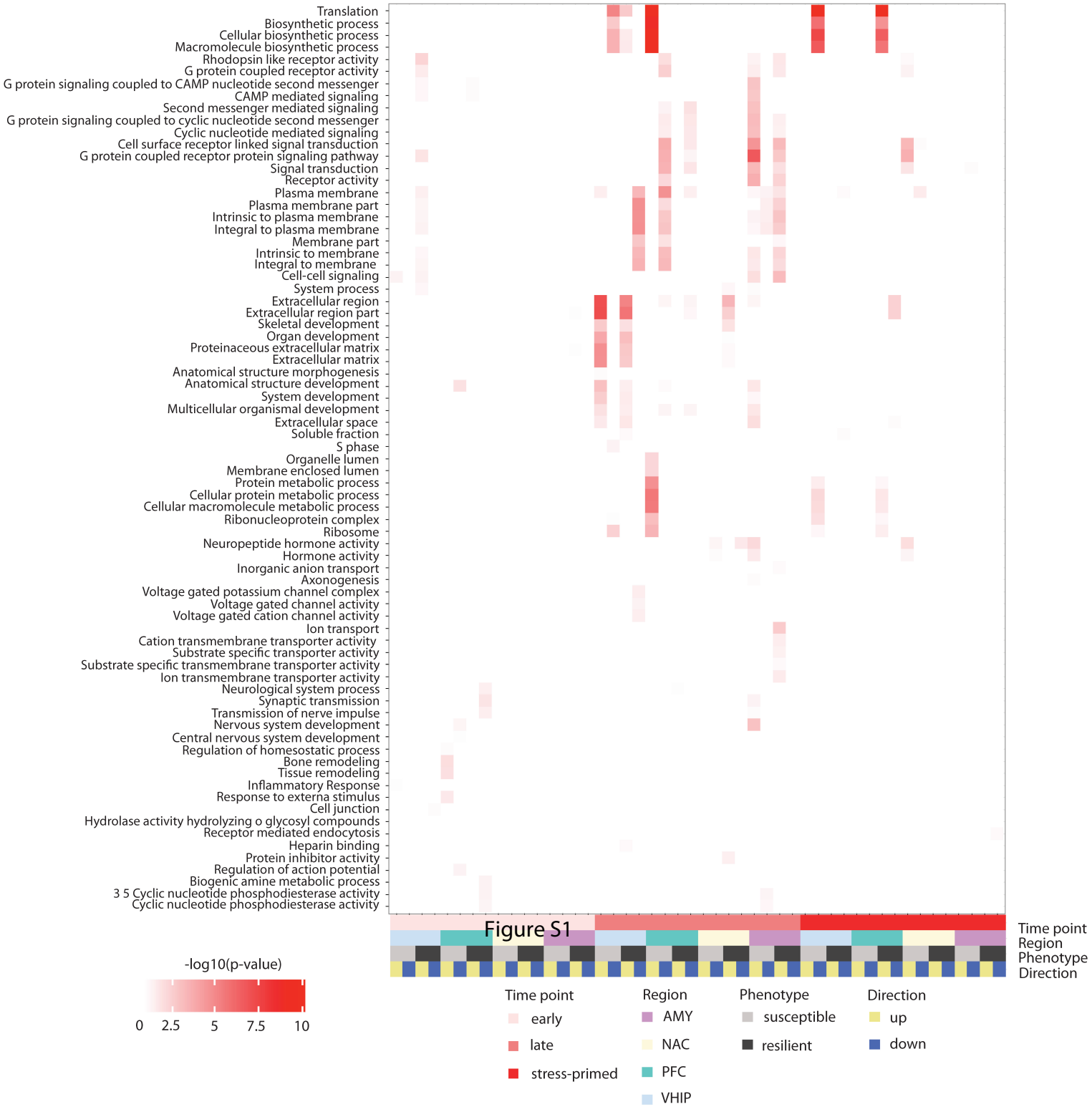
Translation
Biosynthetic process
Cellular biosynthetic process
Macromolecule biosynthetic process
Rhodopsin like receptor activity
G protein coupled receptor activity
G protein signaling coupled to CAMP nucleotide second messenger
CAMP mediated signaling
Second messenger mediated signaling
G protein signaling coupled to cyclic nucleotide second messenger
Cyclic nucleotide mediated signaling
Cell surface receptor linked signal transduction
G protein coupled receptor protein signaling pathway
Signal transduction
Receptor activity
Plasma membrane
Plasma membrane part
Intrinsic to plasma membrane
Integral to plasma membrane
Membrane part
Intrinsic to membrane
Integral to membrane
Cell-cell signaling
System process
Extracellular region
Extracellular region part
Skeletal development
Organ development
Proteinaceous extracellular matrix
Extracellular matrix
Anatomical structure morphogenesis
Anatomical structure development
System development
Multicellular organismal development
Extracellular space
Soluble fraction
S phase
Organelle lumen
Membrane enclosed lumen
Protein metabolic process
Cellular protein metabolic process
Cellular macromolecule metabolic process
Ribonucleoprotein complex
Ribosome
Neuropeptide hormone activity
Hormone activity
Inorganic anion transport
Axonogenesis
Voltage gated potassium channel complex
Voltage gated channel activity
Voltage gated cation channel activity
Ion transport
Cation transmembrane transporter activity
Substrate specific transporter activity
Substrate specific transmembrane transporter activity
Ion transmembrane transporter activity
Neurological system process
Synaptic transmission
Transmission of nerve impulse
Nervous system development
Central nervous system development
Regulation of homesostatic process
Bone remodeling
Tissue remodeling
Inflammatory Response
Response to externa stimulus
Cell junction
Hydrolase activity hydrolyzing o glycosyl compounds
Receptor mediated endocytosis
Heparin binding
Protein inhibitor activity
Regulation of action potential
Biogenic amine metabolic process
3 5 Cyclic nucleotide phosphodiesterase activity
Cyclic nucleotide phosphodiesterase activity
Time point
Region
Phenotype
Direction
-log10(p-value)
0
2.5
5
7.5
10
Time point
early
late
stress-primed
Region
AMY
NAC
PFC
VHIP
Phenotype
susceptible
resilient
Direction
up
down

Figure S1

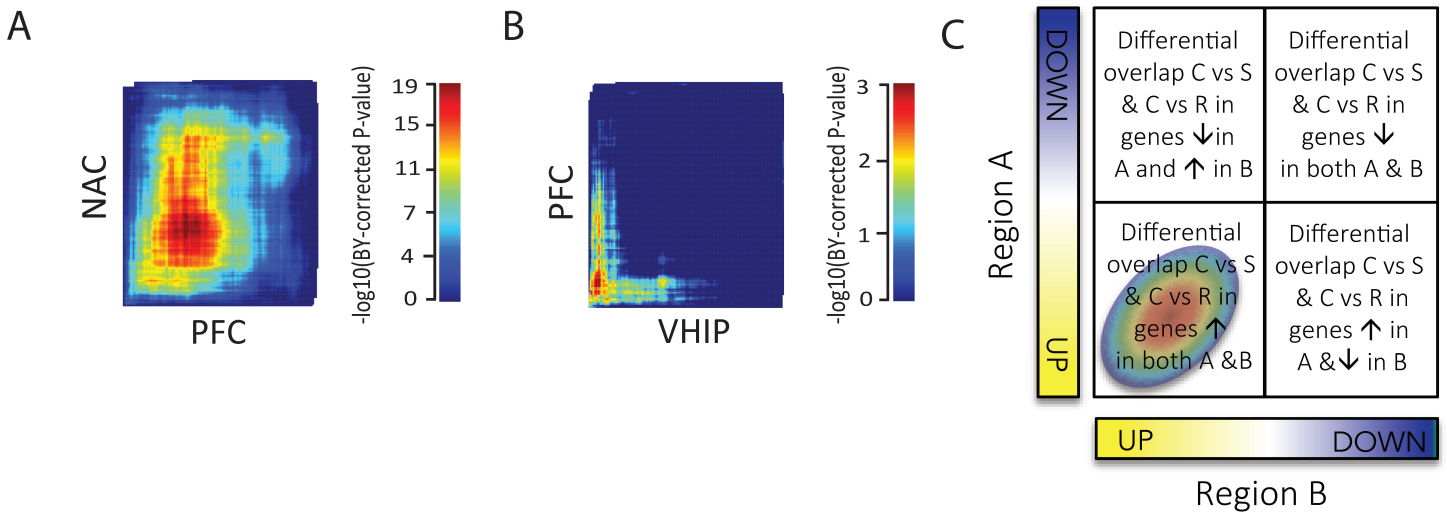
A
NAC
PFC
-log10(BY-corrected P-value)
19
15
11
7
4
0
B
PFC
VHIP
-log10(BY-corrected P-value)
3
2
1
0
C
Region A
DOWN
UP
Differential overlap C vs S & C vs R in genes ↓in A and ↑ in B
Differential overlap C vs S & C vs R in genes ↓ in both A & B
Differential overlap C vs S & C vs R in genes ↑ in both A &B
Differential overlap C vs S & C vs R in genes ↑ in A &↓ in B
UP
DOWN
Region B

Figure S3

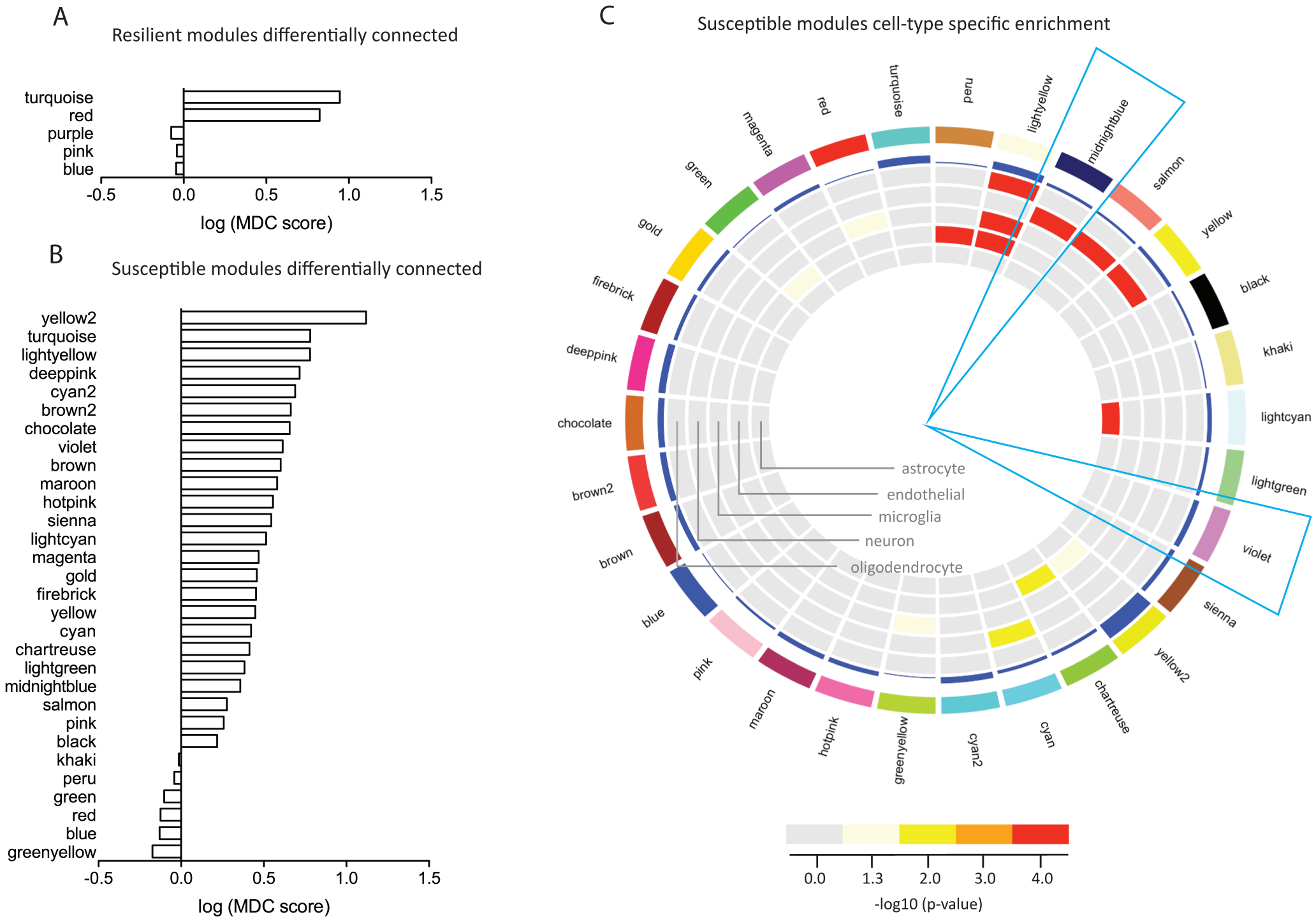
A
Resilient modules differentially connected
turquoise
red
purple
pink
blue
-0.5
0.0
0.5
1.0
1.5
log (MDC score)
B
Susceptible modules differentially connected
yellow2
turquoise
lightyellow
deeppink
cyan2
brown2
chocolate
violet
brown
maroon
hotpink
sienna
lightcyan
magenta
gold
firebrick
yellow
cyan
chartreuse
lightgreen
midnightblue
salmon
pink
black
khaki
peru
green
red
blue
greenyellow
-0.5
0.0
0.5
1.0
1.5
log (MDC score)
C
Susceptible modules cell-type specific enrichment
turquoise
peru
lightyellow
midnightblue
salmon
yellow
black
khaki
lightcyan
lightgreen
violet
sienna
yellow2
chartreuse
cyan
cyan2
greenyellow
hotpink
maroon
pink
blue
brown
brown2
chocolate
deeppink
firebrick
gold
green
magenta
red
astrocyte
endothelial
microglia
neuron
oligodendrocyte
0.0
1.3
2.0
3.0
4.0
-log10 (p-value)

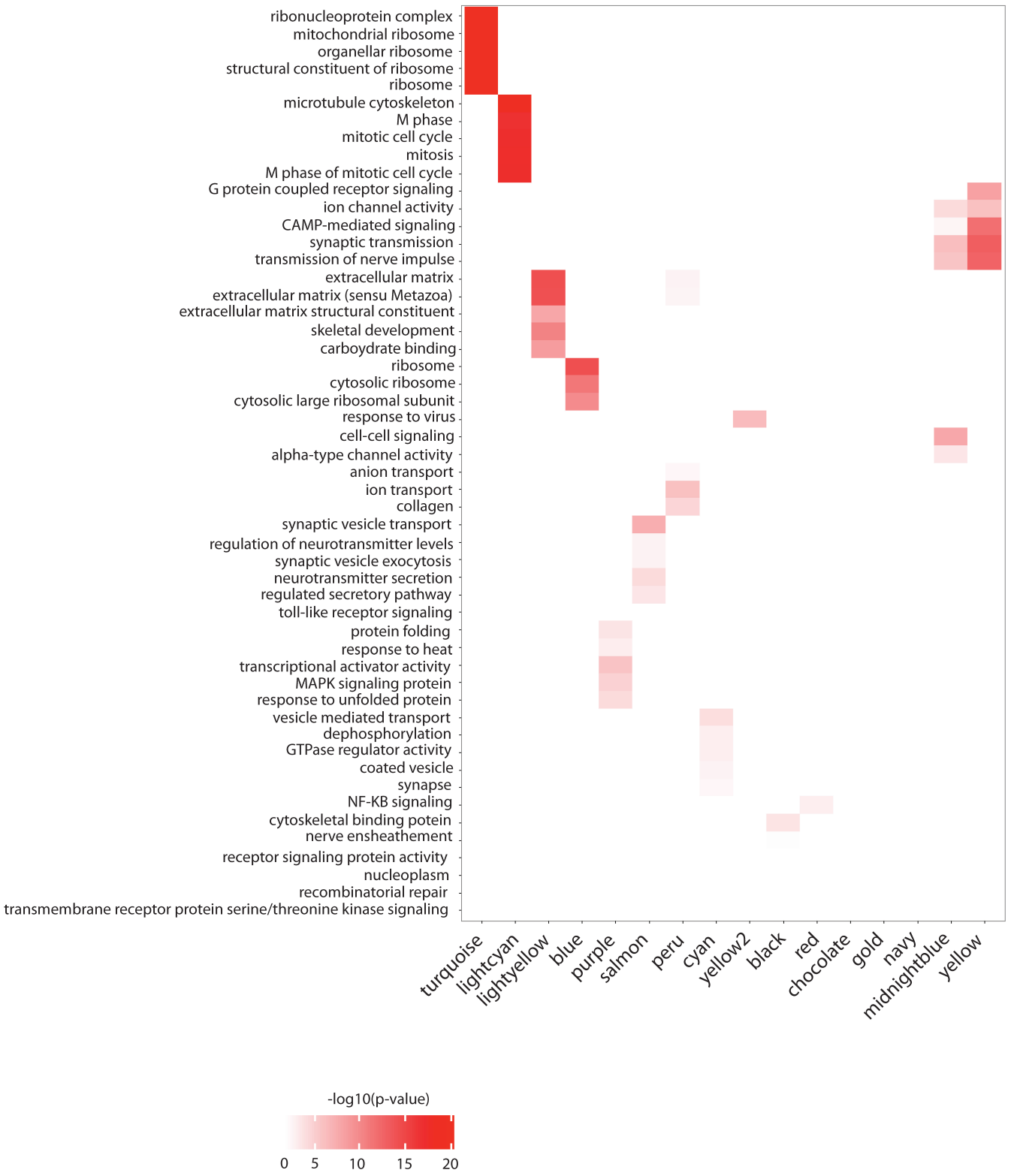
ribonucleoprotein complex
mitochondrial ribosome
organellar ribosome
structural constituent of ribosome
ribosome
microtubule cytoskeleton
M phase
mitotic cell cycle
mitosis
M phase of mitotic cell cycle
G protein coupled receptor signaling
ion channel activity
CAMP-mediated signaling
synaptic transmission
transmission of nerve impulse
extracellular matrix
extracellular matrix (sensu Metazoa)
extracellular matrix structural constituent
skeletal development
carboydrate binding
ribosome
cytosolic ribosome
cytosolic large ribosomal subunit
response to virus
cell-cell signaling
alpha-type channel activity
anion transport
ion transport
collagen
synaptic vesicle transport
regulation of neurotransmitter levels
synaptic vesicle exocytosis
neurotransmitter secretion
regulated secretory pathway
toll-like receptor signaling
protein folding
response to heat
transcriptional activator activity
MAPK signaling protein
response to unfolded protein
vesicle mediated transport
dephosphorylation
GTPase regulator activity
coated vesicle
synapse
NF-KB signaling
cytoskeletal binding potein
nerve ensheathement
receptor signaling protein activity
nucleoplasm
recombinatorial repair
transmembrane receptor protein serine/threonine kinase signaling
turquoise
lightcyan
lightyellow
blue
purple
salmon
peru
cyan
yellow2
black
red
chocolate
gold
navy
midnightblue
yellow
-log10(p-value)
0
5
10
15
20

Figure S5

A

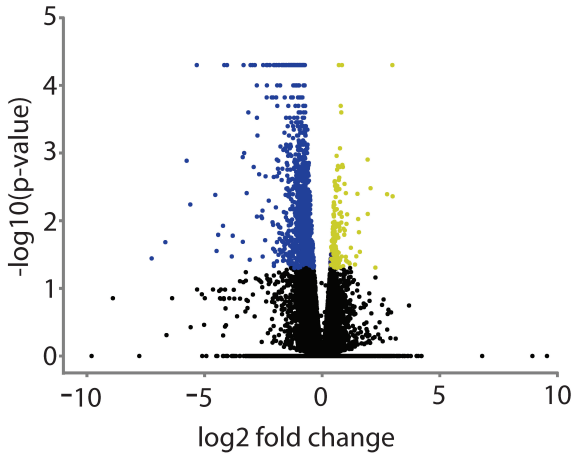
-log10(p-value)
log2 fold change
5
4
3
2
1
0
−10
−5
0
5
10

B

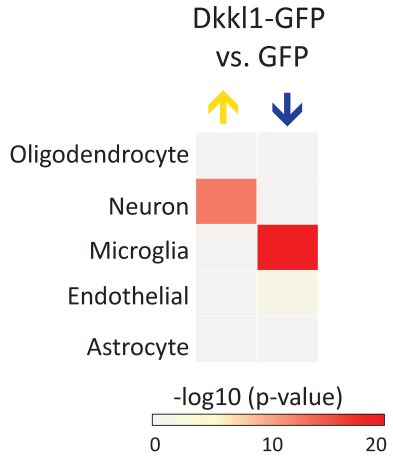
Dkkl1-GFP
vs. GFP
Oligodendrocyte
Neuron
Microglia
Endothelial
Astrocyte
-log10 (p-value)
0
10
20

Figure S6

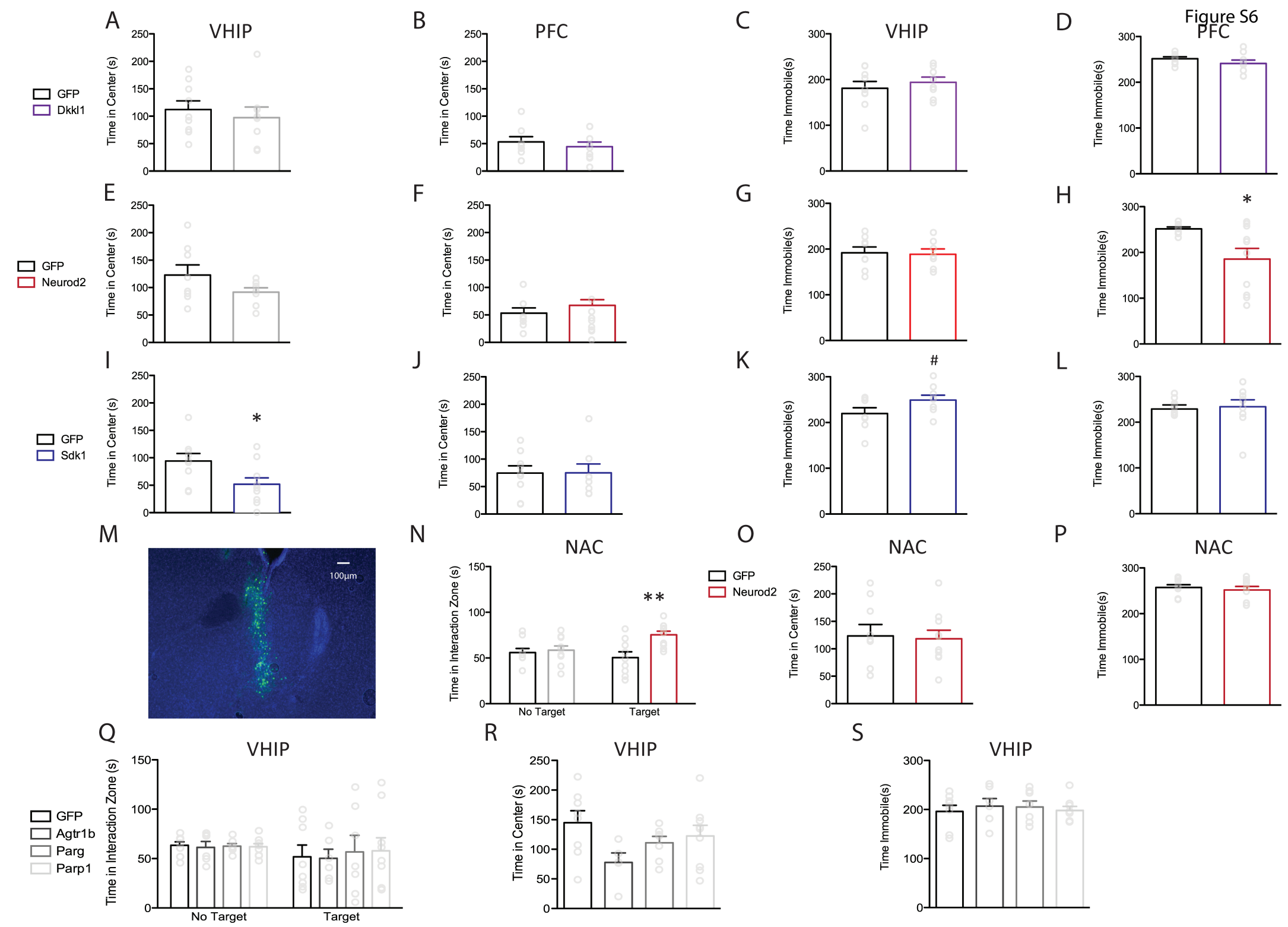
A
VHIP
B
PFC
C
VHIP
D
PFC
GFP
Dkkl1
Time in Center (s)
Time Immobile(s)
E
F
G
H
GFP
Neurod2
*
I
J
K
#
L
GFP
Sdk1
*
M
100µm
N
NAC
**
O
NAC
P
NAC
GFP
Neurod2
Time in Interaction Zone (s)
Time in Center (s)
No Target
Target
Q
VHIP
R
VHIP
S
VHIP
GFP
Agtr1b
Parg
Parp1
Time in Interaction Zone (s)
Time in Center (s)
Time Immobile(s)
No Target
Target

Figure S7

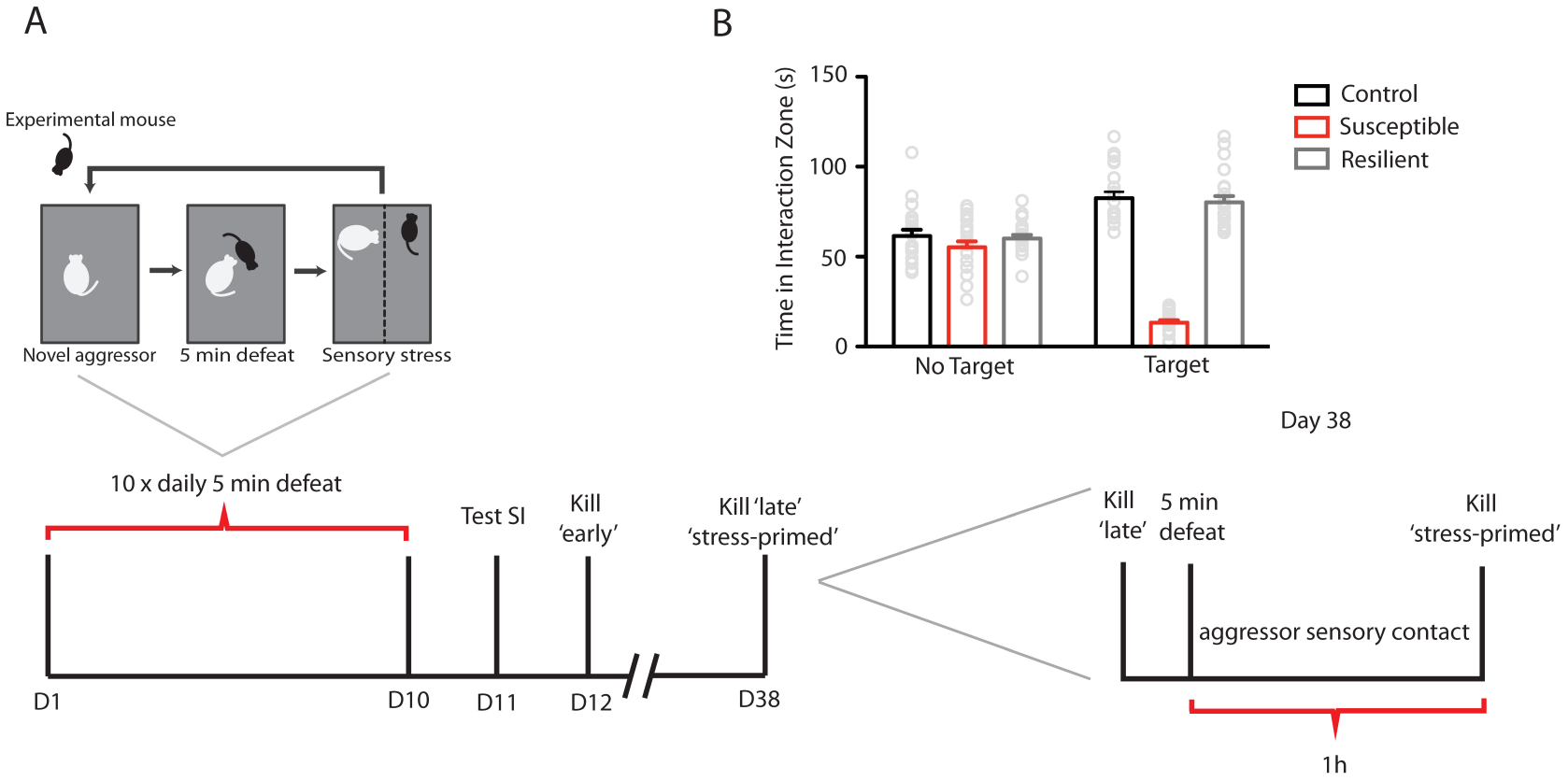
A
Experimental mouse
Novel aggressor
5 min defeat
Sensory stress
10 x daily 5 min defeat
Test SI
Kill 'early'
Kill 'late' 'stress-primed'
D1
D10
D11
D12
D38
B
Time in Interaction Zone (s)
150
100
50
0
Control
Susceptible
Resilient
No Target
Target
Day 38
Kill 'late'
5 min defeat
Kill 'stress-primed'
aggressor sensory contact
1h

Supplementary Figure Legends

Figure S1. *Related to Figure 1*: Gene ontology of differentially expressed genes. Matrix summarizes top gene ontology terms enriched in DEGs upregulated (yellow) and downregulated (blue) in resilient vs. control (dark grey) and susceptible vs. control (light grey), early (48h; light pink), late (28d; dark pink) and stress-primed (28d + 1 h stress; red) after 10 day CSDS in AMY (purple), NAC (cream), PFC (green), and VHIP (lightblue).

Figure S2. *Related to Figure 2*: Rank-rank hypergeometric (RRHO) difference maps determine if susceptible and resilient transcriptomes exhibit significantly different overlap between (A) NAC and PFC and (B) PFC and VHIP by comparing the odds ratio of overlap between brain regions at each pixel. (C) Schematic illustrating interpretation of RRHO difference maps. The results illustrate significant differences in inter-regional coordinated gene regulation in susceptibility vs. resilience.

Figure S3. *Related to Figure 3.* Module differential connectivity analysis and module enrichment for cell-type specific genes. (A) Only 5 resilient modules were significantly differentially connected compared to controls, with 3 modules showing loss of connectivity (logMDC <0, FDR<0 .05) and 2 modules showing gain of connectivity (logMDC >0, FDR<0.05). In contrast, 30 susceptible modules showed differential connectivity compared to controls, with 6 showing loss of connectivity and 24 showing gain of connectivity. (C) Fisher's exact test, corrected for multiple comparisons, determined enrichment for genes with five fold higher expression in oligodendrocytes, neurons microglia, endothelial or astrocytes cell types (Zhang et al., 2014) in significantly differentially connected susceptible modules. Bar color indicates significance of enrichment with increasingly dark colors indicating increasing –log10(p-value).

Figure S4. *Related to Figure 4.* Matrix summarizes top gene ontology terms enriched in susceptible modules. Darker colors indicate increasing –log10(p-value).

Figure S5. *Related to Figure 5.* Cell-type enrichment of differentially expressed genes (DEGs) regulated by *Dkkl1* over-expression. (A) Differential expression analysis identified 108 genes upregulated and 1075 genes downregulated in VHIP in HSV-Dkkl1-GFP vs. HSV-GFP at p<0.05, FC>1.3. (B) Fisher's exact test, corrected for multiple comparisons, determined enrichment for genes with five fold higher expression in oligodendrocytes, neurons microglia, endothelial or astrocytes cell types (Zhang et al., 2014) in significantly differentially connected susceptible modules. Bar color depicts significance of enrichment with increasingly warm colors indicating increasing –log10(p-value). DEGs upregulated by *Dkkl1* over-expression specifically enriched for neuronal genes. DEGs downregulated by *Dkkl1* over-expression enriched for both microglial and endothelial genes.

Figure S6. *Related to Figure 6.* Extended behavioral characterization of the effect of over-expression of susceptible-specific hub-genes. HSV-Dkkl1-GFP injection into ventral hippocampus (VHIP) did not significantly alter time in center time in an open field (OF; A) or immobility in a forced swim test (FST; C). HSV-Neurod2 injection in VHIP decreased center time in OF (E) indicating increased anxiety but did not alter immobility in FST (G). Mice injected with HSV-Sdk1-GFP in VHIP spent less time in the center in OF (I) and showed a trend for increased time immobile in FST (K) than HSV-GFP infected mice indicating increased anxiety and a trend towards increased behavioral despair. No

effects of viral over-expression in prefrontal cortex (PFC) were observed in OF (B, F, J). HSV-Neurod2-GFP in PFC reduced immobility in FST (H) indicating a pro-resilient effect. Neither HSV-Dkkl1-GFP (D) nor HSV-Sdk1-GFP (L) in PFC altered time immobile in FST. (M) Representative image of HSV-GFP expression in NAC. Scale bar = 100μm. (N) Mice injected with HSV-Neurod2-GFP in nucleus accumbens (NAC) spent more time in the interaction zone during a social interaction test compared to HSV-GFP infected mice. The same manipulations did not alter behavior in OF (N) or FST(O). Over-expression in VHIP of genes *not* predicted to induce susceptibility did not alter social interaction (Q), center time in an open field (R) or immobility in FST (S). * $p<0.05$, ** $p<0.01$.

Figure S7. *Related to Methods*: Chronic social defeat stress protocol identifies resilient and susceptible populations. (A) Schematic timeline of CSDS experiments. (B) Social interaction data from a representative CSDS experiment.

Table S1.Differentially expressed genes. *Related to Figure 1*. Lists of differentially expressed genes for susceptible vs. control, resilient vs. control and susceptible vs. resilient VHIP, PFC, NAC and AMY 48h (n=3), 28d (n=4), and 28d + 1h stress (n=4) following 10 day CSDS.

Table S2. Differential gene expression from 48h to 28d. *Related to Figure 1.* Lists of differentially expressed genes in control 28d vs. 48h in VHIP, PFC, NAC and AMY, and intersection between these DEGs and DEGs for susceptible vs. control and resilient vs. control VHIP, PFC, NAC and AMY 48h, 28d, and 28d + 1h stress following 10 day CSDS. The analysis shows that some genes altered by CSDS at the different times points also show age-dependent changes in expression.

Table S3. *Related to Figure 3.* Module summary information for susceptible and resilient WGCNA networks including number of gene members, gene ontology, DEG enrichment and module differential connectivity.

Table S4. *Related to Figure 3*. Validation of weighted gene coexpression network analysis robustness. Module differential connectivity analysis (MDC) of the network constructed on control data (Control MDC) demonstrates that WGCNA is sensitive to detect relatively weak coexpression modules which show gain of connectivity (MDC<1) in susceptibility and resilience. Analysis of module robustness by global conservation rate (GCR) indicates that modules detected in control, susceptible and resilient conditions are highly robust with average GCRs of 98% in susceptible and resilient and 96% in control. Importantly, the MB and V susceptible modules show GCRs of 100%.

Table S5. *Related to Figure 4.* Module information for Midnightblue and Violet susceptible modules including module gene members, hub genes and susceptible-specific hub genes.

Table S6. *Related to Methods.* Cell-type associated lists. Genes expressed at least five-fold higher in one cell type than all other cell types (oligodendrocyte, neuron, microglia, astrocyte, endothelial) using brain-based RNA expression data (Zhang et al., 2014) (http://web.stanford.edu/group/barres_lab/brain_rnaseq.html) used to identify cell-type enrichment.

Extended Experimental Procedures

Experimental subjects

Male 6-8 week-old C57BL/6J mice, and 6-month-old CD1 retired breeders, were maintained on a 12h light-dark cycle (lights on at 7 am) at 22-25° C with *ad libitum* access to food and water. C57BL/6J mice were used as they are a widely used genetically inbred strain facilitating alignment of sequencing data to available genome annotations, detection of experience-dependent transcriptional changes and comparison of our findings to the literature. Mice were housed 5 per cage except following defeat experiments at which point mice were singly housed. All experiments were conducted in accordance with the guidelines of the Institutional Animal Care and Use Committee at Icahn School of Medicine at Mount Sinai. All behavioral testing occurred during the animals' light cycle. Experimenter was blinded to experimental group and order of testing was counterbalanced during behavioral experiments.

CSDS and Behavioral testing

All experiments utilized an established CSDS protocol to induce depressive-like behaviors in mice (Berton et al., 2006; Krishnan et al., 2007). C57BL/6J mice were subjected to 10 daily, 5-min defeats by a novel CD1 aggressor mouse and were then housed across a plexiglass divider to allow for sensory contact for the remainder of the day. Control mice were housed in cages separated from other control mice by a plexiglass divider and were rotated to a different cage daily. Social-avoidance behavior was assessed with a novel CD1 mouse in a two-stage social-interaction test. In the first 2.5-min test (no target), the experimental mouse was allowed to freely explore an arena (44×44cm) containing a plexiglass and wire mesh enclosure (10×6cm) centered against one wall of the arena. In the second 2.5 min test (target), the experimental mouse was returned to the arena with a novel CD1 mouse enclosed in the plexiglass wire mesh cage. Time spent in the 'interaction zone' (14×26cm) surrounding the plexiglass wire mesh cage, 'corner zones' (10×10cm) and 'distance travelled' within the arena was measured by video tracking software (Ethovision 10.0, Noldus). Accelerated social defeat followed a similar protocol except that C57BL/6J were exposed to twice daily, 10-min defeats over the course of four days to coincide with peak viral expression (Dias et al., 2014).

Resilient and susceptible mice were identified by their respective preference for, or avoidance of, interaction with a novel mouse after 10 days of defeat in a social interaction test. To facilitate segregation of phenotypic transcriptional profiles we selected resilient mice according to the following criteria to generate two distinct populations. Resilient mice were defined as mice which spent more time in the interaction zone when the social target was present than absent *and* with total time spent interacting with the social target >60s. Susceptible mice were defined as mice which spent less time in the interaction zone when the social target was present than absent *and* with a total time spent interacting with the social target <30s. (Figure S7). Exploration of an open field arena (44×44cm) was assessed during a 10 min test. A video-tracking system (Ethovision 3.0, Noldus) measured locomotor activity, as well as the time spent in the center (34×34cm) and periphery of the test arena as an index of anxiety. For the forced swim test, mice were individually placed in beakers of 25°C water for 6 min. Immobility was assessed by a video-tracking system (Ethovision 3.0, Noldus).

RNA isolation

Mice were killed directly from their home-cage 48h (early) or 28d (late) after CSDS or 28d after CSDS and 1h after a 5min re-exposure to an aggressor (stress-primed), brains were removed, coronally sliced and VHIP, PFC, NAC and AMY tissues were rapidly dissected and frozen on dry ice. Tissue from 3-5 mice were pooled for each sample to reduce biological variability without increasing library number. Sample sizes of for n=3 (early) or n=4 (late, stress-primed) independent biological replicates for each brain region, phenotype and time-point are consistent with published studies using RNA-seq analysis of microdissected brain tissue.

RNA isolation, qPCR and data analyses were performed as described previously (Bagot et al., 2015). Briefly, total RNA was isolated with TriZol reagent (Invitrogen) and purified with RNAeasy micro kits from Qiagen. All RNA samples were determined to have 260/280 and 260/230 values ≥1.8.

For viral-manipulation experiments, mice were injected with HSV-Dkkl1-GFP or HSV-GFP alone in ventral hippocampus (VHIP). Following 24h recovery from surgery, mice were exposed to 2 x daily 10 minute aggressive encounters for 4 days, and were housed in the cage of an aggressive mouse separated by a plexi-glass divide. 24 h after the final defeat mice were killed and bilateral VHIP tissue punched to isolate RNA and prepare libraries from individual mice.

RNA-sequencing and library preparation

RNA integrity was assessed using either an Agilent 2100 Bioanalyzer with the RNA 6000 Nano assay or an Agilent 2200 TapeStation with the R6K ScreenTape (Agilent, Santa Clara, CA). Average RIN values were above 9. Libraries were prepared using the TruSeq RNA Sample Prep Kit v2 protocol (Illumina, San Diego, CA). Briefly, the cDNA was synthesized from poly-A-selected and then fragmented total RNA using random hexamers, followed by end-repair and ligation with sequencing adaptors. The libraries were then size selected and purified using AMPure XP beads (Beckman Coulter, Brea, CA). Barcode bases (6 bp) were introduced at one end of the adaptors during PCR amplification steps. Library size and concentration were measured by Bioanalyzer or Tape Station (Life Technologies, Grand Island, NY) before sequencing. Libraries were sequenced on the Illumina HiSeq 2500 System utilizing V3 chemistry with 100 base pair single-end reads at the Mount Sinai Genomics Core Facility. For viral manipulation experiments, libraries were sequenced on Illumina HiSeq 2500 System utilizing V4 chemistry with125 bp single-end reads at Beckman Coulter.

Statistical and bioinformatic data analysis

Differential expression analyses

Sequencing short reads were aligned to the mouse mm9 reference transcriptome using Tophat (Trapnell et al., 2009). Read count normalization and gene expression estimation were done by Cufflinks (Trapnell et al., 2012). We first filtered for protein-coding and long non-coding genes and then performed pairwise differential expression analysis with Cuffdiff (Trapnell et al., 2012) using the negative binomial distribution. A nominal significance threshold of $p<0.05$ and fold change >1.3 was used.

RRHO

We applied a rank rank hypergeometric overlap test (RRHO) to compare patterns of gene regulation between pairs of brain regions of susceptible and resilient mice at 48h

post-defeat. RRHO identifies overlap between expression profiles in a threshold free manner to assess the degree and significance of overlap (Plaisier et al., 2010).
Full differential expression lists were ranked by the -log10(p-value) multiplied by the sign of the fold change from the Cuffdiff analysis. The Rank Rank Hypergeometric Overlap test (RRHO) was used to evaluate the overlap of differential expression lists between pairs of brain regions (Plaisier et al., 2010; Stein et al., 2014). A one-sided version of the test only looking for over-enrichment was used. RRHO difference maps were produced for pairs of RRHO maps (resilient vs. control and susceptible vs. control) by calculating for each pixel the normal approximation of difference in log odds ratio and standard error of overlap between resilient vs. control and susceptible vs. control. This Z score was then converted to a P-value and corrected for multiple comparisons across pixels (Benjamini and Yekutieli, 2001).

Coexpression network analyses

In order to identify differences in gene-gene correlations between the three treatment groups (C, S and R) and discover group-specific correlation structures, we employed a group-specific network analysis (Zhang et al., 2013). The susceptible and resilient data sets (each n= 44) from 21,850 expressed genes were independently processed through weighted gene coexpression network analysis (WGCNA) (Langfelder et al., 2008; Zhang and Horvath, 2005). (Note that this is substantially greater than the recommended samples size for coexpression network analysis (20; https://labs.genetics.ucla.edu/horvath/CoexpressionNetwork/Rpackages/WGCNA/faq.html).The weighted network analysis began with a matrix of the Pearson correlations between all gene pairs, and then converted the correlation matrix into an unsigned adjacency matrix using a power function, so that the resulting adjacency matrix, i.e., the weighted coexpression network, is approximately scale-free. To explore the modular structures of the coexpression network, the adjacency matrix was further transformed into a topological overlap matrix (Zhang and Horvath, 2005). Because topological overlap between two genes reflects both their direct interaction and their indirect interactions through all other genes in the network, this approach helps create more cohesive and biologically more meaningful modules. To identify modules of highly co-regulated genes, we used average linkage hierarchical clustering to group genes based on the topological overlap of their connectivity, followed by a dynamic cut-tree algorithm to dynamically cut clustering dendrogram branches into gene modules. To distinguish between modules, each module was assigned a unique, arbitrary color identifier. Coexpression analysis exploits variability within gene expression data to extract functionally important coexpression (co-regulation) relationships among genes; data from multiple time-points and brain regions harbor a variety of perturbations of key pathways underlying susceptibility and resilience, thus enhancing the power to detect robust co-regulation. In an unbiased manner, WGCNA identifies clusters (modules) of coexpressed genes, which may reflect common biological functions (Langfelder et al., 2008; Zhang and Horvath, 2005).

Overrepresentation of gene ontologies (GOs) in modules was assessed through Fisher's exact test corrected for multiple testing using MSigDB (Broad Institute; http://www.broadinstitute.org/gsea/msigdb/index.jsp). To assess cell-type specificity we curated lists (Table S5) of genes expressed at least five-fold higher in one cell type than all other cell types (neuron, microglia, astrocyte, oligodendrocyte, endothelial) using brain-based RNA expression data (Zhang et al., 2014)

(http://web.stanford.edu/group/barres_lab/brain_rnaseq.html) and used Fisher's exact test corrected for number of modules and cell-types tested to determine significance of enrichment. We used the Benjamini-Hochberg empirical false discovery rate (FDR 0.05) method, which constrains the overall rate of false positive events, to control for multiple testing (Benjamini-Hochberg, 1995).

To quantify differences in transcript network organization between susceptible and control and resilient and control mice, we employed a modular differential connectivity (MDC) metric (Zhang et al., 2013). In brief, MDC is the ratio of the connectivity of all gene pairs in a module from susceptible or resilient mice, to that of the same gene pairs from control mice. MDC is a continuous measure ranging from 0 to infinity. MDC >1 indicates gain of connectivity or enhanced co-regulation between genes, whereas MDC <1 indicates loss of connectivity or reduced co-regulation between genes. The statistical significance of the MDC metrics was computed by a permutation test. The significance or FDR of the MDC statistic can be assessed by permuting the data underlying the two networks. We estimated FDR based both on shuffled samples (i.e., networks with nonrandom nodes but random connections) and shuffled gene labels (i.e., networks with random nodes but nonrandom connections), and then selected the larger value as the final FDR estimate.

To further identify key hub (or driver) genes of the modules identified by WGCNA, we applied key driver analysis (Zhang et al., 2013) to the module-based unweighted coexpression networks derived from ARACNe (Algorithm for the Reconstruction of Accurate Cellular Networks) (Margolin et al., 2006). ARACNe was used first to identify significant interactions between genes in each module based on their mutual information, with indirect interactions then removed through data processing inequality (DPI). For each ARACNe-derived unweighted network, we further identified the hub genes by examining the number of N-hob neighborhood nodes (NHNN) for each gene. A gene's NHNNs are the nodes within N-hobs (layers) from the gene. For a given network, let μ be the numbers of NHNNs for all genes. Genes with number of NHNNs greater than $\overline{\mu} + \sigma(\mu)$ are nominated as hubs (Zhang et al., 2013). This criterion identified key hub genes with a number of NHNNs significantly above the corresponding average value. To identify whether key driver genes were unique to the susceptible condition, we determined whether identified hub genes would attain hub gene status in hypothetical modules constructed from control transcriptional profiles on the same network of genes. Genes identified as key drivers in susceptible and not in the corresponding control networks were termed susceptible-specific hub genes.

To formally assess the robustness of the modules in each network, we performed coexpression network analysis on a number of sets of randomly selected samples (85% of the total) in each group. Twenty networks from 20 sets of randomly selected samples in each of the control, resilient and susceptible groups were constructed and then compared with the modules based on the full-size data of the corresponding group. A module (*m*) in the full-size data of the group (*X*) is considered to be conserved in the coexpression network from a set of randomly selected samples (*Y*) if *m* significantly overlaps at least one module in the data *Y* based on a threshold of 0.05 for the Bonferroni-corrected p values. A module's conservation rate (MCR) is defined as the percentage of the networks in which the module is conserved. The global conservation rate (GCR) for all the modules in a full-sized network is the average of MCRs of all

modules in that network. All networks were highly robust. Specifically, Midnightblue and Violet modules are 100% conserved (Supplementary S4).

Stereotaxic surgery and viral vectors

For *in vivo* behavioral validation, mice were injected with HSV vectors and following 48h recovery from surgery, mice were exposed to 2 x daily 10 minute aggressive encounters for 4 days, and were housed in the cage of an aggressive mice separated by a plexi-glass divide. Social interaction (SI) behavior was tested 24h after the final defeat in a two part test in which mice first explored an arena with an empty wire mesh enclosure on one wall (No Target) and then explored the same arena in the presence of a novel social target (Target) contained within the wire mesh enclosure.

We over-expressed genes of interest using bicistronic p1005 herpes-simplex viral (HSV) vectors expressing GFP alone or GFP plus *Sdk1*, *Neurod2* or *Dkkl1*. In this system, GFP expression is driven by a cytomegalovirus (CMV) promoter, while the gene of interest is driven by the IEF4/5 promoter. For stereotaxic surgeries, mice were anesthetized with a mixture of ketamine (100 mg/kg) and xylazine (10 mg/kg) and positioned in a small-animal stereotaxic instrument (Kopf Instruments). The skull surface was exposed and 33-gauge syringe needles (Hamilton) were used to bilaterally infuse 0.5 µl HSV virus at a rate of 0.1 µl/min into mPFC (bregma coordinates: anterior/posterior, 1.7 mm; medial/lateral, 0.75 mm; dorsal/ventral, -2.5 mm ; 15° angle), vHIP (bregma coordinates: anterior/posterior, -3.7 mm; medial/lateral, 3 mm; dorsal/ventral, -4.8 mm; 0° angle) or NAC (bregma coordinates: anterior/posterior, -1.6 mm; medial/lateral, -1.5 mm; dorsal/ventral, -4.7 mm; 10° angle).

For electrophysiology experiments 0.75ul of virus was infused at a rate of 0.25ul/min.

Electrophysiology

24h after viral infusion, mice were deeply anesthetized with isoflurane and decapitated. Coronal slices (250µm thick) containing the ventral subiculum subregion of the VHIP (Bregma -3.4 to -4.2 mm) were cut in ice-cold sterile cutting solution (135 mM N-methyl-d-glucamine, 1 mM KCl, 1.2 mM KH2PO4, 0.5 mM CaCl2, 1.5 mM MgCl2, 20 mM choline-HCO3, 11 mM glucose, pH = 7.4, saturated with 95% O2 /5% CO2).
K-based internal solution was used (in mM): 130 potassium methanesulfate, 10 KCl, 10 HEPES, 0.4 EGTA, 2.0 MgCl2, 2.5 MgATP, 0.25 Na3GTP, pH 7.3–7.4; 290–295 mOsm. Slices were incubated at room temperature for 1-2h prior to recording. The recording bath contained (in mM) 126 NaCl, 1.6 KCl, 1.2 NaH2PO4, 1.2 MgCl2, 2.5 CaCl2, 18 NaHCO3, and 11 glucose, and equilibrated at 30–31 °C with 95% O2/5% CO2 (290-295 mOsm), with 100 µM picrotoxin. Data were collected using Clampex (Molecular Devices). First whole-cell patch was achieved under voltage clamp at -70 mV and then switched to current clamp mode. Under current clamp mode, neurons were held at -70 mV, and pulsed with 300 ms current at 200 pA to characterize the firing pattern of neurons (burst vs. regular firing). After returning to voltage clamp mode, synaptic currents were recorded in gap-free mode, filtered at 2 kHz, amplified five times, and then digitized at 20 kHz with a Digidata 1440A analog-to-digital converter (Molecular Devices). Spontaneous EPSCs were recorded for 3-5min as the precedent current-clamp recording of action potentials precluded the use of TTX. Recordings were analyzed using Clampfit (Molecular Devices).

Supplemental References

Benjamini, Y., and Hochberg, Y. (1995). Controlling the false discovery rate- a practical and powerful approach to multiple testing. Journal of the Royal Statistical Society Series B- Statistical Methodology. 289-300.
Benjamini, Y., and Yekutieli, D. (2001). The control of the false discovery rate in multiple testing under dependency. Annals of Statistics. *29*, 1165-1188.
Trapnell, C., Pachter, L., and Salzberg, S.L. (2009). TopHat: discovering splice junctions with RNA-Seq. Bioinformatics *25*, 1105-1111.